Biointerface Research in Applied Chemistry
Platinum Open Access Journal (ISSN: 2069-5837)

Article
Volume 11, Issue 4, 2021, 12215 - 12226
https://doi.org/10.33263/BRIAC114.1221512226

Effect of Ce-Mn Codoping on the Structural, Morphological and Electrical Properties of the $BaTiO_3$ Based Ceramics

Tahmida Iqbal [1], Myeesha Mostafa [2], Md Saif Ishtiaque [3], Mohammad Jellur Rahman [4*], Shamima Choudhury [1]

[1] Department of Physics, University of Dhaka, Dhaka-1000, Bangladesh; email: tahmidaraheen@gmail.com (T.I.), skc.phy@gmail.com (S.C.);
[2] Department of Physics, Jagannath University, Dhaka-1100, Bangladesh; email: myeesha0811@yahoo.com (M.M.);
[3] Department of Physics, University of Barishal, Barishal-8200, Bangladesh; email: ishtiaque.phy@gmail.com (S.I.);
[4] Department of Physics, Bangladesh University of Engineering and Technology, Dhaka-1000, Bangladesh; email: mjrahman@phy.buet.ac.bd (M.J.R.);
* Correspondence: mjrahman@phy.buet.ac.bd (M.J.R);

Scopus Author ID 55457930700

Received: 3.12.2020; Revised: 27.12.2020; Accepted: 29.12.2020; Published: 3.01.2021

Abstract: Undoped, Cerium (Ce) doped, Manganese (Mn) doped and Ce-Mn co-doped Barium Titanate ($BaTiO_3$) with the general formula $Ba_{1-x}Ce_xMn_yTi_{1-y}O_3$ (where x = 0.00, 0.01, 0.02, 0.03, y = 0.00; x = 0.00, y =0.01, 0.02, 0.03; and x = y = 0.01, 0.02,0.03) were synthesized by solid-state reaction method and sintered at 1200 °C for 4 hr with an aim to study their structural and electrical properties. The grain size of the samples has been estimated using the Scanning Electron Microscopy (SEM). The X-ray Diffraction (XRD) analysis indicates that the structure of the Ce-doped and Ce-Mn co-doped $BaTiO_3$ is cubic. However, the undoped $BaTiO_3$ and Mn-doped $BaTiO_3$ confirmed the tetragonal-cubic mixed phases. With the change of doping concentrations, the positions of different peaks shifted slightly. The lattice parameter varied irregularly with increasing doping concentration because of Mn's changeable valency. EDX spectra confirmed the presence of Ba, Ti, Ce, and Mn contents in the co-doped samples with stoichiometric ratio. Crystallinity is observed to be clearly increased when Ce-Mn is co-doped in $BaTiO_3$. *J-V* characteristic curves indicate transition from conducting to semiconducting nature for the doped and co-doped samples with the increase in temperature. The dielectric constant of the samples increases up to 4500 with the doping concentration. The higher values of dielectric constant are observed for the 2% Mn-doped and 1% Ce-Mn co-doped samples compared to the other undoped samples. For the undoped and Mn-doped samples, constant dielectric values increase with temperature but decrease for the Ce-doped and Ce-Mn co-doped samples. It is inferred that co-doping of $BaTiO_3$ with Ce and Mn would be beneficial and economical for its applications.

Keywords: barium titanate; co-doping; SEM; XRD; electrical properties; dielectric constant.

1. Introduction

Ceramic is a branch of art and science in which solid materials are essentially composed of inorganic, nonmetallic materials. Among all the applications of ceramics, use as a dielectric is remarkable. Excellent dielectric, ferroelectric and piezoelectric properties are the reasons for using barium titanate ($BaTiO_3$) in diverse applications [1-2]. $BaTiO_3$ has a perovskite structure. Because of its elevated dielectric constant, it is frequently used in fabricating electronic elements such as MLCs, PTC thermistors, and piezoelectric transducers. Pure $BaTiO_3$ is an

insulator, whereas it transforms into a semiconductor in contact with doping. Apart from PTCR properties, $BaTiO_3$ as a semiconductor is applied in sensor applications [3]. It can also increase the dielectric constant of microwave absorbing materials [4]. The most conventional procedure to enhance dielectric, electrical, and magnetic properties is to dope this ABO_3 perovskite system [5-6]. Partial substitution of other materials in $BaTiO_3$ has been done to improve the temperature stability of permittivity. Change in the crystal structure is possible by doping other ions if they are not too different in size of Ba^{2+} or Ti^{4+} ions. The conductivity of rare earth element (Cerium) doped $BaTiO_3$ increases with dopant concentration [7]. Lattice deformation might occur when the $BaTiO_3$ is doped with the transition metals. Kirianov *et al*. have reported that doping with Manganese would promote the transition from the tetragonal to cubic phases[8]. Tetragonal to tetragonal-cubic mixed-phase and finally cubic phase can occur with increasing sintering temperature [9]. A/B site doping in ABO_3 perovskite and extension of the solid solution with another member is proven as a potential candidate for a better capacitor [10]. The orientation of electrical polarization in $BaTiO_3$, which is related to the electronic core level and valance band, shift to higher energy [11].

Resistivity, dielectric constant, and dielectric loss factors are important parameters for electric insulators and circuits. In this research work, these properties have been studied at different temperatures. The structural and electrical characteristics of $BaTiO_3$ have a significant influence on Ce and Mn doping. This research aims to study the effect of doping and co-doping on the structural and electrical properties of $BaTiO_3$ ceramics at different temperatures and to compare these properties with undoped $BaTiO_3$.

2. Materials and Methods

Solid-state reaction method has been applied to prepare undoped, doped and co-doped $BaTiO_3$ with the general formula of $Ba_{1-x}Ce_xMn_yTi_{1-y}O_3$ (where for pure $BaTiO_3$ x = 0.00, y = 0.00; for Ce doped samples x = 0.01, 0.02, 0.03; y = 0.00, for Mn-doped samples x = 0.00; y = 0.01, 0.02, 0.03 and for Ce-Mn co-doped x = y = 0.01, 0.02, 0.03). To prepare the ceramic composite, oxide powders such as BaO, TiO_2, CeO_2, and MnO_2, are collected from Merck, Germany, each having purity 98% and weighted precisely after screening mixed. These powders were ground for 15 min by an agate mortar pestle. Then, to form a homogenous blend, they were ball milled with distilled water using zirconium balls of radius 0.5 cm for 6 hours. This ground liquid was kept still for 24 hr so that precipitation can occur, and then a Bunsen burner was used to dry them. The dried samples were then again ground for 1.5 hr to form a powder. The powders were calcined at 700 °C (6 °C/min) for 2 hrs in a Nabertherm furnace (Model HT 16/18, Germany), and then the temperature of the furnace was decreased at the rate of 3 °C/min. Afterward, the samples were grounded for 15 min, and 0.93 gm of such powders are binded by 2% polyvinyl alcohol to form pellets of diameter 1.2 cm and thickness 0.175 cm by pressing by a uniaxial hydraulic press (Model HERZOG HTP 40, series no- MA 14822-1-1, Germany) with a force of 40 kN. Samples were sintered at 1200 °C for four hours with a heating rate of 6 °C/min and a cooling rate of 3 °C/min. After sintering, the pellets were smoothed with brown flint paper. A scanning electron microscope (SEM, Hitachi S-3400N, Japan) was employed to observe the samples' surface morphology and average grain size. An X-ray diffractometer (Model Rigaku Ultima IV, Japan) was used to investigate the structural property. For electrical measurement, silver liquid of high conductivity was pasted on each

face of the pellets. Finally, Wayne Kerr 6500B series Precision Impedance Analyzer (Bognor Regis, UK) has been used to analyze the ceramics' dielectric properties.

3. Results and Discussion

3.1. X-ray diffraction analysis.

Solid-state synthesis is the most conventional method, which produces relatively agglomerated and coarse particles [12].

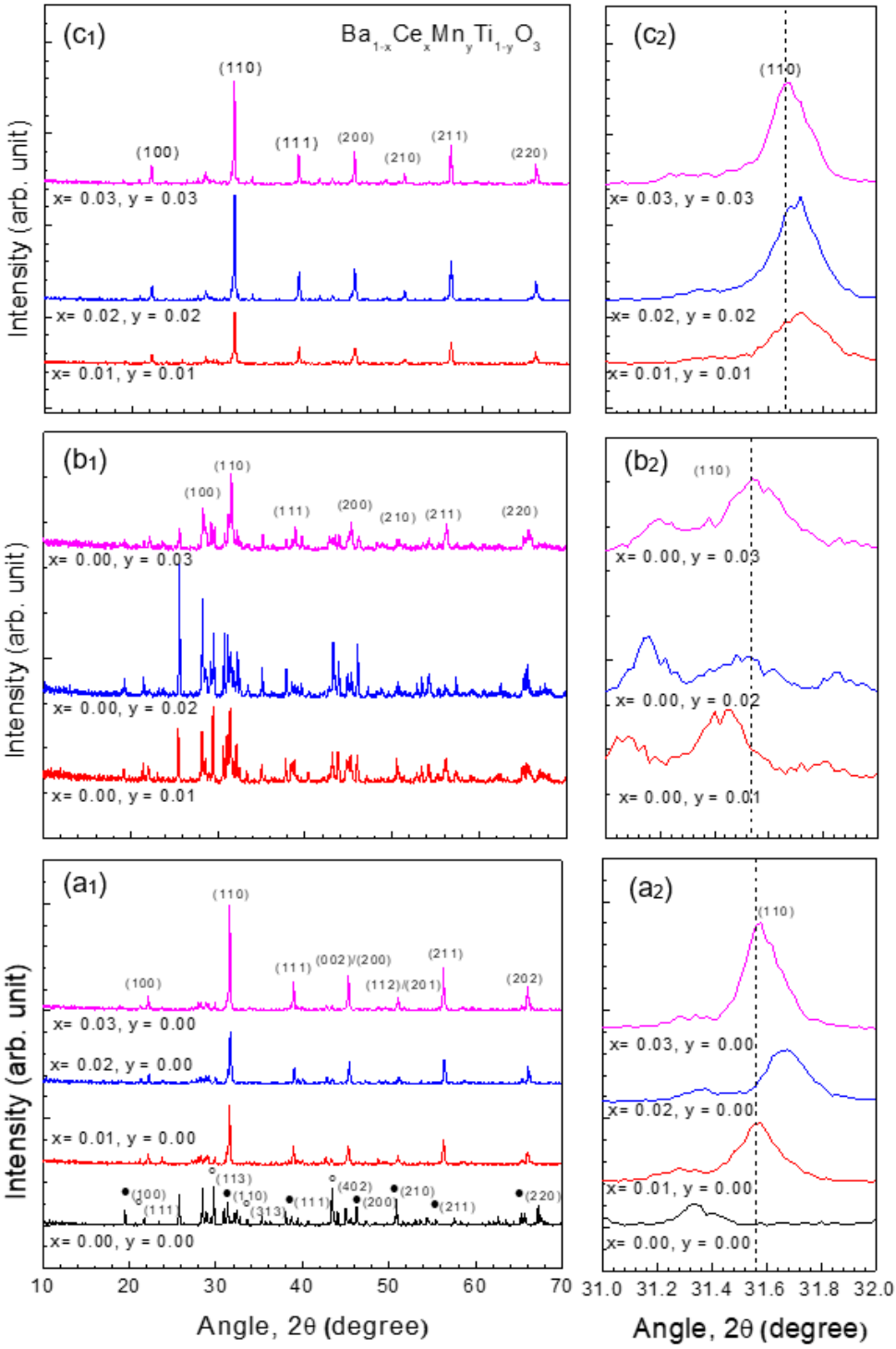

Figure 1. X-ray difrraction spectra (a_1, b_1, c_1) and shiffting of the (110) peak (a_2, b_2, c_2) for (a_1, a_2) pure (x,y = 0.00) and Ce-doped (x = 0.01 to 0.03, y = 0.00), (b_1, b_2) Mn-doped (x = 0.00, y = 0.01 to 0.03), (c_1, c_2) Ce-Mn co-doped (x,y = 0.01 to 0.03) $BaTiO_3$.

In this study, it is observed that though $BaTiO_3$ has a pure structural phase the doped and co-doped samples have a mixture of $BaTiO_3$ and $BaTi_2O_5$ phases, which was identified by the XRD pattern as shown in Fig. 1. For undoped and Ce-doped $BaTiO_3$, it is noticed that with increasing concentration of dopants, the XRD pattern got smoother, and the intensity of the peak increases. Figures 1(b1) and 1(c1) show the XRD pattern for the Mn-doped and Ce-Mn co-doped $BaTiO_3$ samples. It is observed that with increasing concentration of the dopants, the XRD patterns got smoother too. In the doped samples, the peaks for the $BaTi_2O_5$ phase are less, which indicates the reduction of impurities. Previous studies showed that the XRD patterns of the undoped $BaTiO_3$ have a single peak at 45° corresponding to (002) Miller index when it is in the cubic phase. It offers a peak splitting at 45° corresponding to (002) and (020) peaks for the tetragonal phase [13-14]. Indication of pseudo-cubic perovskite structure in the tetragonal phase was also observed in previous studies of $BaTiO_3$ based ceramics [15]. It was reported that doping concentration has an important relation between the sintering temperature and tetragonality [16].

In some cases, splitting of the peaks has been observed in pure $BaTiO_3$ and 1%, 2% Mn-doped $BaTiO_3$ as shown in Figs. 1(a_2) and 1(b_2). Whereas, 3% of the Mn-doped $BaTiO_3$ shows the nature of the cubic-tetragonal mixed phase, indicating the possibility of phase transition in the higher doping concentration of Mn. Previously, Suravi *et al*. also found cubic-tetragonal mixed-phase compositions in Mn-doped $BaTiO_3$ [17]. It is observed that (110) peak shifted toward a larger angle when Ce or Mn is doped in pure $BaTiO_3$. In Ce-doped $BaTiO_3$, this happened because Ce^{3+} of ionic radius 0.102 nm is lighter and occupies the place of heavier Ba^{2+} (ionic radius 0.135 nm) [18-19]. The ionic radius of Ti^{4+} (0.0745 nm) is larger than that of Mn^{4+} (0.064 nm), causing the right shift of the $BaTiO_3$ peak. Because of additives' nature, XRD peaks of the Ce-Mn co-doped samples also shifted towards the right. The peak intensities increased with a doping concentration in Ce-doped and Mn-doped $BaTiO_3$. Phase shift was very slight in the Ce-Mn co-doped $BaTiO_3$, but peak intensities were increased significantly in these co-doped samples. D-spacing and lattice parameter is related to the peak shift. The smoothest peak was observed for the co-doped samples. The intensity of the major peak increases with Ce and Mn's addition, which indicates better crystallization of the samples [14]. From the major peaks lattice parameters, *a* were calculated by using the Nelson-Riley method using the equation

$$F(\theta) = \frac{1}{2}\left(\frac{cos^2\theta}{sin\theta} + \frac{cos^2\theta}{\theta}\right)$$

and are presented in Table 1.

The lattice parameter is observed to be changed randomly with an increase in doping concentration. Mn's changeable valance can be a reason for these irregular values because valency variation can impact dielectric, ferroelectric, and piezoelectric properties [20]. For Ce doped and Ce-Mn co-doped $BaTiO_3$, the lattice parameter decreases slightly with increasing doping concentration. As Mn-doped $BaTiO_3$ has a mixed cubic-tetragonal phase, it has different values of lattice parameters. It is observed that the lattice parameter, *c*, decreases with increasing Mn concentration but *a* shows an irregular variation of value with a concentration of doping. The Debye-Scherrer equation has been used to determine crystallite sizes. A higher ratio of *c*/*a* for the Mn-doped $BaTiO_3$, when x = 0.02, confirmed the improved tetragonality of the sample. This result supports the previously reported data where Sandeep *et al*. also observed improved tetragonality for Pb-doped $BaTiO_3$ [21]. The cubic-tetragonal mixed phase is

responsible for the ferroelectric and dielectric properties of the samples [22]. When x = 0.02, Mn-doped $BaTiO_3$ shows the highest *c*/*a* ratio.

Owing to the Ce doping, initially crystallite size of the samples decrease from that of the pure $BaTiO_3$, but with the increase of doping concentration, crystallite size increased. However, the change in crystallite size is irregular for different doping concentrations of Mn. After that, crystallite size decreases again with the increase in doping concentration. This finding agrees with the findings described in Refs. [23-24]. Ce and Mn co-doped $BaTiO_3$ showed smaller crystallite sizes than that of the pure $BaTiO_3$, but with increasing dopant concentration, the crystallite sizes increase linearly [24-25]. Zali *et al*. studied that the crystallite size of BaTiO3 increases with tetragonality and sintering temperature [26]. Because of the decrease in tetragonality with doping, crystallite sizes decrease for the Ce and Ce-Mn co-doped samples, where x = 0.01 in the general formula. As Mn-doped $BaTiO_3$ is in the tetragonal phase up to x = 0.02, the tetragonality decrease with a doping concentration of Mn, indicating the reduction in crystallite size. Tetragonality is reduced owing to the decrease of grain sizes and increment of measurement temperature [27].

3.2. Scanning electron microscope analysis.

Surface morphology and microstructures of the ceramic sample for different amounts of Ce and Mn in $BaTiO_3$ were studied by SEM images, which are shown in Fig. 2. Irregular grain sizes and intergranular pores of various sizes have been observed by the SEM analysis. This type of irregularly shaped pores and grains without curving have also been reported in CuO doped $BaTiO_3$-$PbTiO_3$ [28]. It is noticed that with the addition of Mn, the grain sizes of the samples decreased. Sitko *et al*. observed similar characteristics for the Mn-doped $BaTiO_3$ in their research work [29]. Grain size of around 0.5 µm is observed for the pure $BaTiO_3$ pellet [30-31]. In this research, the grain sizes showed consistency with the lattice parameter for Ce-Mn co-doped samples but varied irregularly for Ce-doped and Mn-doped compositions. Because Mn is a transition metal, when doped in $BaTiO_3$, the sample shows both ferroelectric and ferromagnetic properties [32]. Studies showed that variation of electric properties has no relation with the grain sizes, phase, and domain structure may have sensitivity with doping content, and different Mn doping concentration has no relation with grain sizes [33-34].

Table 1. Different parameters were obtained from the XRD and SEM studies of the $Ba_{1-x}Ce_xMn_yTi_{1-y}O_3$ samples.

$Ba_{1-x}Ce_xMn_yTi_{1-y}O_3$		Lattice Parameter		Crystallite size (nm)	Grain Size (nm)
		a (Å)	*c* (Å)		
x = 0.00	y = 0.00	3.97	4.11	68.16	0.507
x = 0.01	y = 0.00	4.00	4.00	60.20 60.2	0.828
x = 0.02	y = 0.00	4.00	4.00	60.10	0.709
x = 0.03	y = 0.00	3.99	3.99	71.02	0.949
x = 0.00	y = 0.01	4.02	4.01	43.01	0.431
x = 0.00	y = 0.02	3.93	4.00	15.50	0.547
x = 0.00	y = 0.03	4.02	3.97	38.00	0.413
x = 0.01	y = 0.01	3.99	3.99	45.11	0.405
x= 0.02	y = 0.02	3.99	3.99	58.13	0.386
x = 0.03	y = 0.03	3.99	3.99	69.36	0.569

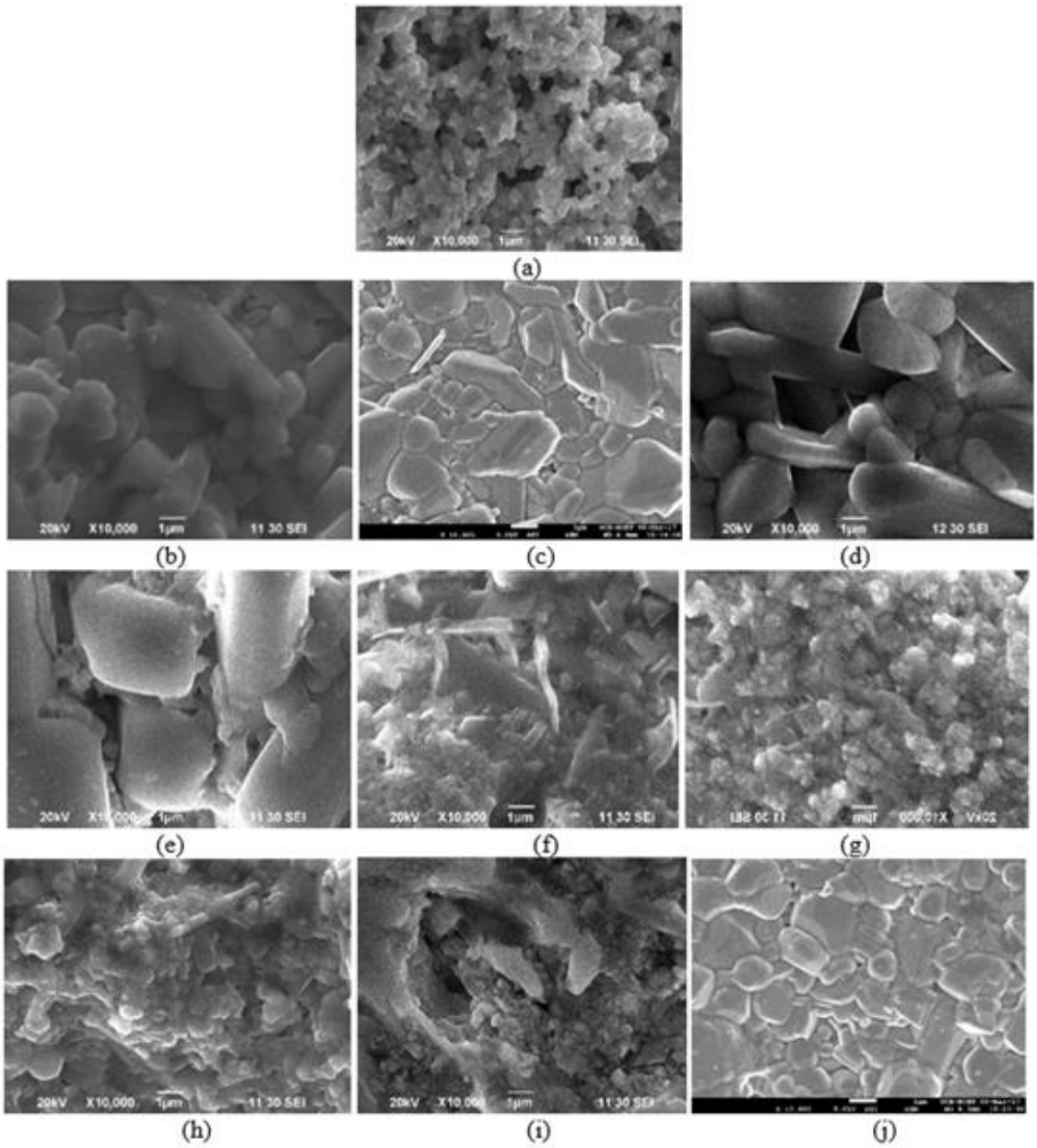

Figure 2. SEM images of $Ba_{1-x}Ce_xMn_yTi_{1-y}O_3$ for (a) x = y = 0.0, (b) x = 0.01, y = 0.0, (c) x = 0.02, y = 0.0, (d) x = 0.03, y = 0.0, (e) x = 0.0, y = 0.01, (f) x = 0.0, y = 0.02, (g) x = 0.0, y = 0.03, (h) x = y = 0.01, (i) x = y = 0.02 and (j) x = y = 0.03.

3.3. Energy dispersive X-ray analysis.

In the EDX spectrum, as shown in Fig. 3, the existence of X-ray peaks for Ce and Mn for the co-doped sample indicates the presence of Ce and Mn with a nominal perovskite phase. Ce and Mn-rich regions also do not reveal any impurity content. The difference in microstructural features is also associated with Ce and Mn's inhomogeneous distribution, as seen in the EDX spectra taken from different areas in the same sample. Mn-doped $BaTiO_3$ is in the cubic-tetragonal mixed phase, whose tetragonality decreases with Mn doping. A reduction in crystallite size has been observed.

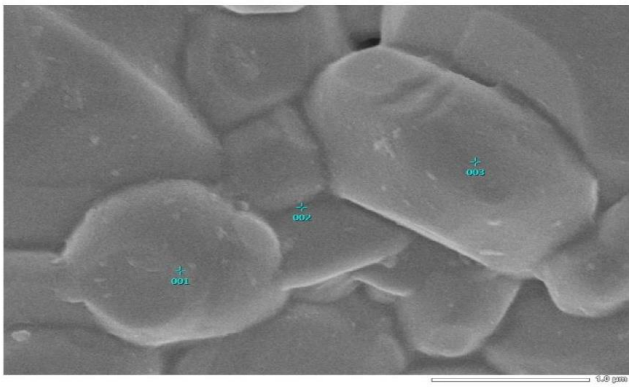

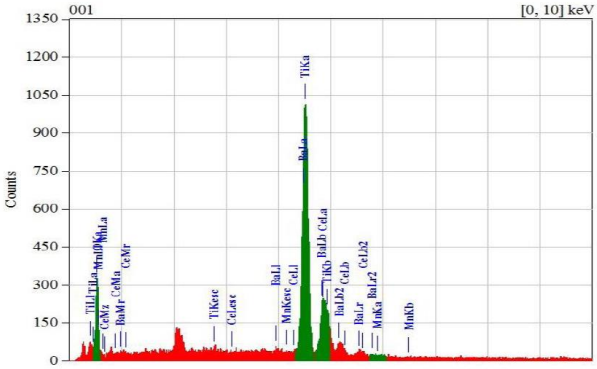

Element		(keV)	Mass%	Sigma	Atom%
O K		0.525	8.96	0.19	28.91
Ti K		4.508	52.19	0.62	56.28
Mn K	*	5.894	0.53	0.17	0.50
Ba L		4.464	24.90	0.81	9.37
Ce L		4.837	13.42	0.61	4.95
Total			100.00		100.00

Figure 3. EDX analysis of $Ba_{1-x}Ce_xMn_yTi_{1-y}O_3$ with x = y = 0.03.

3.4. Variation of current density with temperature.

The *J-V* characteristics of all the undoped, doped, and co-doped samples are shown in Fig. 4. Samples showed approximate Ohmic nature at the lower temperatures [35], however current density show an increasing trend with the increase in temperature. In this research, current density and temperature increment are proportional, and the highest value of *J* was observed at 125 °C. It is also observed that with the doping initially, the current density increases very sharply but decreases with the content of doping for each case. The charge transfer between the layers of the sample exhibited nonlinear behavior and is considered responsible for the inverse piezoelectric effect in the heterostructure [36].

3.5. Temperature-dependent DC resistivity and dielectric constant.

It is observed that the DC resistivity of all the samples starts to increase around 120°C, as shown in Fig. 5(a). For undoped and 1%, 2% Mn-doped $BaTiO_3$, resistivity decreases initially but starts to increase around 120 °C, which indicates a conductor-semiconductor phase transition among these samples. Previously, Rao *et al*. investigated that the increment of DC electrical resistivity above Curie temperature can occur due to the trapped holes on Ba-O bonds, contributing to hole conduction [37].

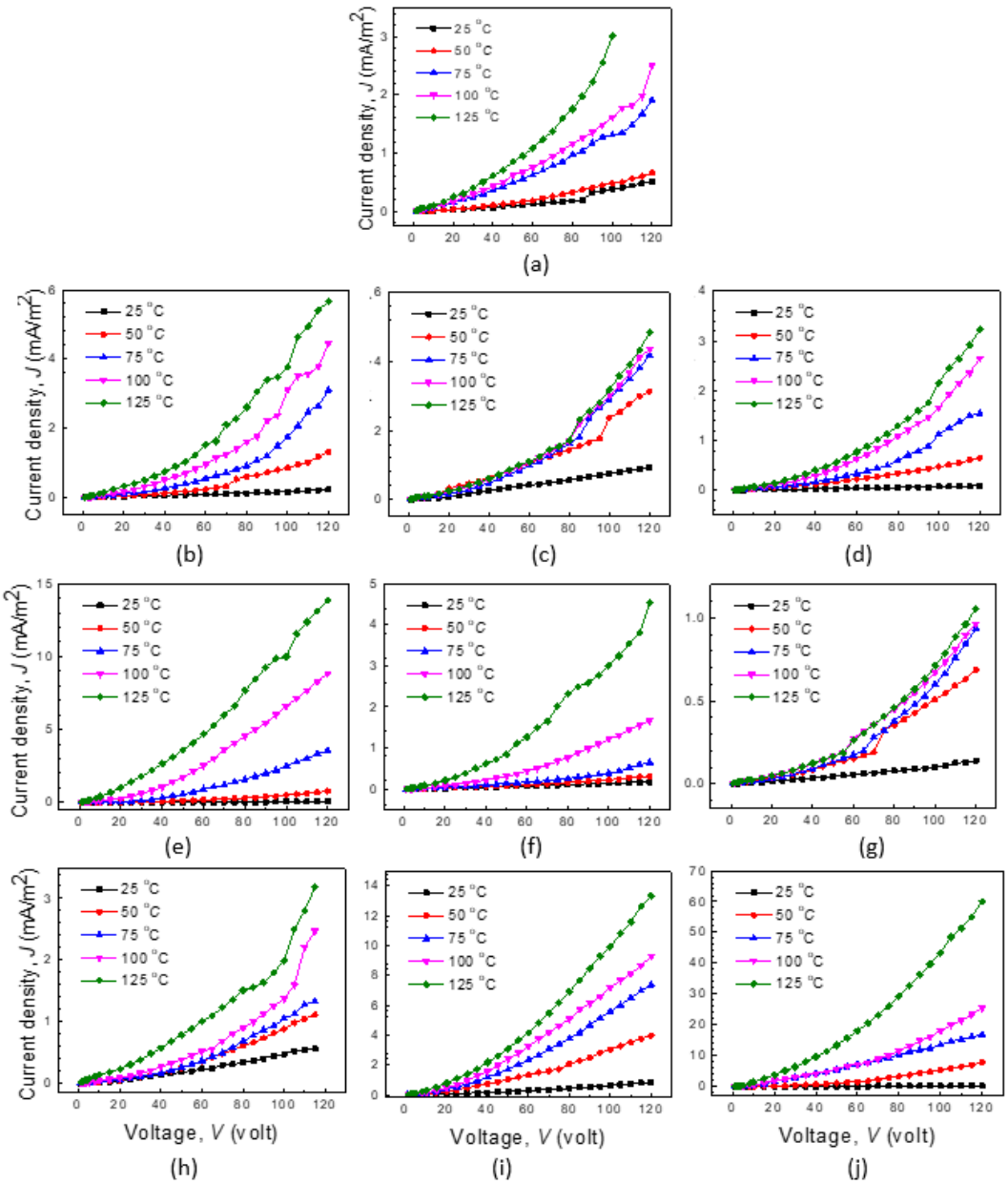

Figure 4. *J-V* characteristic curves of (a) pure, (b-d) Ce-doped, (e-g) Mn-doped and (h-j) Ce-Mn co-doped $BaTiO_3$, where (a) x = 0.00, y = 0.00, (b) x = 0.01, y = 0.00, (c) x = 0.02, y = 0.00, (d) x = 0.03, y = 0.00, (e) x = 0.00, y = 0.01, (f) x = 0.00, y = 0.02, (g) x = 0.00, y = 0.03, (h) x = 0.01, y = 0.01, (i) x = 0.02, y = 0.02, and (j) x = 0.03, y = 0.03 in $Ba_{1-x}Ce_xMn_yTi_{1-y}O_3$.

Figure 5 (a) shows a decrease in resistivity with increasing temperature for the undoped and Mn-doped $BaTiO_3$ samples, confirming the semiconducting nature. However, for Ce doped and Ce-Mn co-doped $BaTiO_3$, resistivity increases with increasing temperature, i.e., a sample showing conducting nature. 1% Ce-Mn co-doped $BaTiO_3$ shows irregular values. The lowest resistivity has been observed for 3% Ce-Mn co-doped $BaTiO_3$. The highest resistivity has been observed for undoped $BaTiO_3$ at room temperature, indicating better semiconductive nature in Ce-Mn co-doped $BaTiO_3$ with increasing doping concentration. The temperature-dependent resistivity, though studied for the samples sintered at various temperatures and Sr-doped $BaTiO_3$, the initial decrease of resistivity in pure and Mn-doped $BaTiO_3$ has a good match with previous works [32-35].

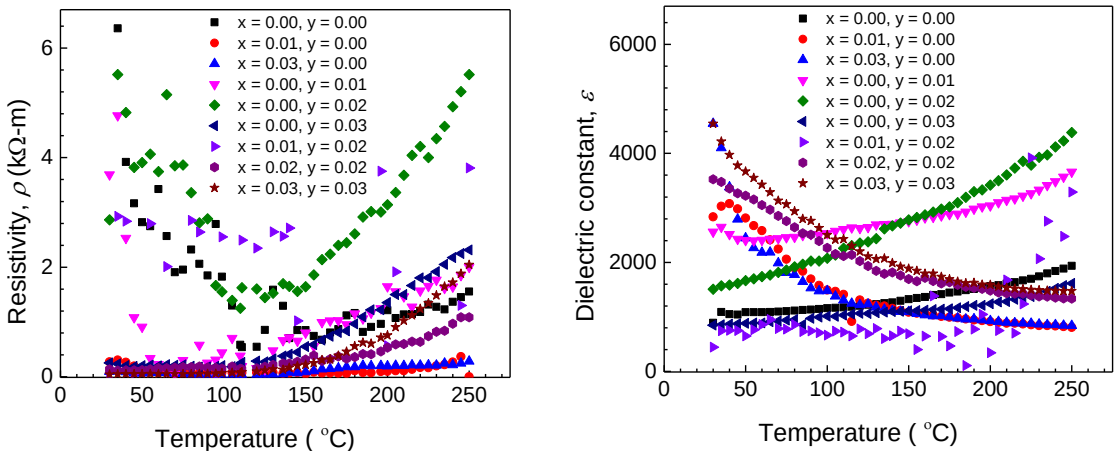

(a) (b)

Figure 5. Temperature dependent (a) DC resistivity and (b) dielectric constant of the Ce-doped, Mn-doped and Ce-Mn co-doped $BaTiO_3$ with composition $Ba_{1-x}Ce_xMn_yTi_{1-y}O_3$.

The effect of microstructure on the dielectric properties of all the compositions as a function of temperature was studied and is shown in Fig. 5 (b). The dielectric constant for the undoped and Mn-doped $BaTiO_3$ samples observed to be increased with increasing temperature, but for the Ce-doped and Ce-Mn co-doped $BaTiO_3$ samples decreases significantly with temperature. The highest dielectric constant has been observed for the co-doped sample of x = y = 0.03. A slight transition has been observed around 50 °C for 1% Ce doped and 1% Mn-doped $BaTiO_3$ samples. The absence of Curie temperature in this study indicates a phase transition may occur less than 0 °C, which was also reported to be possible in other studies [23,32,38,39]. Therefore, the study of the samples under room temperature could be important, which will be done in the near future. Previously, Bosman *et al*. studied that the constant dielectric increases with temperature when its value is low, but for a higher value of dielectric constant, it changes inversely with temperature because the dielectric properties depend on the grain size the samples [38,39]. Moreover, this sample's dielectric properties may also depend on the frequency range and annealing temperature [40]. The variation of dielectric loss for the different compositions matches previous studies [41-42].

The dielectric loss of all the compositions varies between 0.01 – 0.1 with the increase in temperature. But 1% Ce-Mn co-doped $BaTiO_3$ gave anomalous dielectric loss values. In this composition, Mn's concentration is considered dominant, which might cause this unstable electrical property. With a higher concentration of co-doping, samples showed more Ce dominant results. 3% Ce-Mn co-doped $BaTiO_3$ shows good dielectric characteristic at room temperature; however, the samples' dielectric properties with 2% of Mn doping in $BaTiO_3$ seemed promising at a higher temperature. Owing to the high dielectric constant and low dielectric loss, the co-doped sample could be the best candidate as a high-performance dielectric material [43].

4. Conclusions

Crystallite sizes of the $Ba_{1-x}Ce_xMn_yTi_{1-y}O_3$ showed irregular shape for most compositions, but Ce-Mn co-doping indicates a significant effect on the crystallite sizes. XRD pattern confirmed the tetragonal phase for the undoped $BaTiO_3$ and tetragonal-cubic mixed phase for the Mn-doped $BaTiO_3$. Ce-doped and Ce-Mn co-doped samples showed a cubic phase and reduced impurity for the sample with higher doping concentration. All the samples

at the low voltage region showed approximate Ohmic nature with low conductivity, but at the higher voltages, they showed semiconducting behavior. A transition from conductor to semiconductor has been observed in the temperature-dependent DC electrical resistivity graph. The dielectric behavior of the Ce-doped and Ce-Mn co-doped $BaTiO_3$ samples show opposite characteristics to one another. In terms of stability and electrical properties, the 2% Mn-doped $BaTiO_3$ gave the best results. This sample showed the highest dielectric constant (about 4500) and the lowest dielectric loss with the increment of temperature. Whereas undoped $BaTiO_3$ shows a dielectric constant of only about 1000. At 1% Ce-Mn co-doped samples, an irregular pattern of electrical properties has been observed, but with a higher doping concentration of Ce and Mn, the sample follows the characteristic of Ce rather than Mn. Because Ce is a rare earth element, co-doping of $BaTiO_3$ with Ce and Mn would be beneficial and economical.

Funding

This research received no external funding.

Acknowledgments

The authors would like to acknowledge the support of the Department of Physics, University of Dhaka, and the assistance of the Department of Physics, Department of Glass and Ceramic Engineering of the Bangladesh University of Engineering and Technology, Dhaka, Bangladesh, during the research.

Conflicts of Interest

The authors declare no conflict of interest.

References

1. Su, J.; Zhang, J. Recent development on modification of synthesized barium titanate (BaTiO3) and polymer/BaTiO3 dielectric composites. *Journal of Materials Science: Materials in Electronics* **2019**, *30*, 1957-1975, https://doi.org/10.1007/s10854-018-0494-y.
2. Popescu, D.G.; Husanu, M.A.; Chirila, C.; Pintilie, L.; Teodorescu, C.M. Impact on Ferroelectricity and Band Alignment of Gradually Grown Au on BaTiO3. *physica status solidi (RRL) – Rapid Research Letters* **2019**, *13*, https://doi.org/10.1002/pssr.201900077.
3. Ertuğ, B. The Overview of the Electrical Properties of Barium Titanate. *American Journal of Engineering Research* **2013**, *2*, 01-07.
4. Akinay, Y.; Hayat, F. Synthesis and microwave absorption enhancement of BaTiO3 nanoparticle/polyvinylbutyral composites. *Journal of Composite Materials* **2018**, *53*, 593-601, https://doi.org/10.1177/0021998318788144.
5. Chan, H.M.; Harmer, M.R.; Smyth, D.M. Compensating Defects in Highly Donor-Doped BaTiO3. *Journal of the American Ceramic Society* **1986**, *69*, 507-510, https://doi.org/10.1111/j.1151-2916.1986.tb07453.x.
6. García, S.; Font, R.; Portelles, J.; Quiñones, R.J.; Heiras, J.; Siqueiros, J.M. Effect of Nb Doping on (Sr,Ba)TiO3 (BST) Ceramic Samples. *Journal of Electroceramics* **2001**, *6*, 101-108, https://doi.org/10.1023/A:1011496414921.
7. Issa, M.A.A.; Molokhia, N.M.; Dughaish, Z.H. Effect of cerium oxide (CeO2) additives on the dielectric properties of BaTiO3ceramics. *Journal of Physics D: Applied Physics* **1983**, *16*, 1109-1114, https://doi.org/10.1088/0022-3727/16/6/019.
8. Kirianov, A.; Ozaki, N.; Ohsato, H.; Kohzu, N.; Kishi, H. Studies on the Solid Solution of Mn in BaTiO3. *Japanese Journal of Applied Physics* **2001**, *40*, 5619-5623, https://doi.org/10.1143/jjap.40.5619.
9. Funsueb, N.; Limpichaipanit, A.; Ngamjarurojana, A. Electrical properties and microstructure of phase combination in BaTiO3-based Ceramics. *Journal of Physics: Conference Series* **2018**, *1144*, https://doi.org/10.1088/1742-6596/1144/1/012133,
10. Wang, D.; Wang, G.; Murakami, S.; Fan, Z.; Feteira, A.; Zhou, D.; Sun, S.; Zhao, Q.; Reaney, I.M. BiFeO3-BaTiO3: A new generation of lead-free electroceramics. *Journal of Advanced Dielectrics* **2018**, *08*, https://doi.org/10.1142/S2010135X18300049.

11. Oshime, N.; Kano, J.; Ikenaga, E.; Yasui, S.; Hamasaki, Y.; Yasuhara, S.; Hinokuma, S.; Ikeda, N.; Janolin, P.-E.; Kiat, J.-M.; Itoh, M.; Yokoya, T.; Fujii, T.; Yasui, A.; Osawa, H. Skewed electronic band structure induced by electric polarization in ferroelectric BaTiO3. *Scientific Reports* **2020**, *10*, https://doi.org/10.1038/s41598-020-67651-w.
12. Bouharras, F.E.; Raihane, M.; Ameduri, B. Recent progress on core-shell structured BaTiO3@polymer/fluorinated polymers nanocomposites for high energy storage: Synthesis, dielectric properties and applications. *Progress in Materials Science* **2020**, *113*, https://doi.org/10.1016/j.pmatsci.2020.100670.
13. Lee, H.-W.; Moon, S.; Choi, C.-H.; Kim, D.K. Synthesis and Size Control of Tetragonal Barium Titanate Nanopowders by Facile Solvothermal Method. *Journal of the American Ceramic Society* **2012**, *95*, 2429-2434.
14. Liu, Q.; Liu, J.; Lu, D.; Li, T.; Zheng, W. Dense Sm and Mn Co-Doped BaTiO3 Ceramics with High Permittivity. *Materials* **2019**, *12*, https://doi.org/10.3390/ma12040678.
15. Lv, J.; Hao, H.; Jiang, X.; Liu, Z.; Emmanuel, M.; Cao, M.; Yao, Z.; Liu, H. Defect structure evolution and electrical properties of BaTiO3-based ferroelectric ceramics. *Journal of the American Ceramic Society* **2020**, *103*, 5129-5138, https://doi.org/10.1111/jace.17220.
16. Kholodkova, A.; Smirnov, A.; Danchevskaya, M.; Ivakin, Y.; Muravieva, G.; Ponomarev, S.; Fionov, A.; Kolesov, V. Bi2O3-Modified Ceramics Based on BaTiO3 Powder Synthesized in Water Vapor. *Inorganics* **2020**, *8*, https://doi.org/10.3390/inorganics8020008.
17. Islam, S.; Siddika, A.; Khatun, N.; Hossain, M.; Hosney, M.; Begum, M.; Ahmed, N. Structural, Dielectric and Electric Properties of Manganese-Doped Barium Titanate. *International Journal of Nanoelectronics and Materials* **2018**, *11*.
18. Hwang, J.H.; Han, Y.H. Electrical Properties of Cerium-Doped BaTiO3. *Journal of the American Ceramic Society* **2001**, *84*, 1750-1754, https://doi.org/10.1111/j.1151-2916.2001.tb00910.x.
19. Ramesh, M.N.V.; Ramesh, K.V. Effect of cerium substitution on structural and impedance properties of 0.8Ba0.2(Bi0.5K0.5)TiO3 lead free ceramic system. *Modern Physics Letters B* **2016**, *30*, https://doi.org/10.1142/S0217984916500561.
20. Chen, J.; Cheng, J.; Guo, J.; Cheng, Z.; Wang, J.; Liu, H.; Zhang, S. Excellent thermal stability and aging behaviors in BiFeO3-BaTiO3 piezoelectric ceramics with rhombohedral phase. *Journal of the American Ceramic Society* **2020**, *103*, 374-381, https://doi.org/10.1111/jace.16755.
21. Butee, S.; Kambale, K.R.; Ghorpade, A.; Halikar, A.; Gaikwad, R.; Panda, H. Significant improvement in Curie temperature and piezoelectric properties of BaTiO3 with minimum Pb addition. *Journal of Asian Ceramic Societies* **2019**, *7*, 407-416, https://doi.org/10.1080/21870764.2019.1656359.
22. Baji, A.; Mai, Y.-W. Effect of barium titanate reinforcement on tensile strength and dielectric response of electrospun polyvinylidene fluoride fibers. In: *Novel Aspects of Nanofibers*. InTech; **2018**; https://doi.org/10.5772/intechopen.74662.
23. Rahman, S.N.; Khatun, N.; Islam, S.; Ahmed, N.A. Comparative studies of cerium and zirconium doped barium titanate. *Int J Emerg Technol Comput Appl Sci*. **2014,** *14*.
24. Kumar, Y.; Mohiddon, M.; Srivastava, A.; Yadav, K.L. Effect of Ni doping on structural and dielectric properties of BaTiO3. *Indian Journal of Engineering and Materials Sciences* **2009**, *16*, 390-394.
25. Choudhury, S.; Akter, S.; Rahman, M.J.; Bhuiyan, M.A.; Khatun, N.; Hossain, M. Structural, Dielectric and Electrical Properties of Zirconium Doped Barium Titanate Perovskite. *Journal of Bangladesh Academy of Sciences* **2009**, *32*, https://doi.org/10.3329/jbas.v32i2.2434.
26. Zali, N.M.; Mahmood, C.S.; Mohamad, S.M.; Foo, C.T.; Murshidi, J.A. X-ray diffraction study of crystalline barium titanate ceramics. *AIP Conference Proceedings* **2014**, *1584*, 160-163, https://doi.org/10.1063/1.4866124.
27. Yoon, S.-H.; Kim, M.-Y.; Kim, D. Correlation between tetragonality (c/a) and direct current (dc) bias characteristics of BaTiO3-based multi-layer ceramic capacitors (MLCC). *Journal of Materials Chemistry C* **2020**, *8*, 9373-9381, https://doi.org/10.1039/d0tc02067b.
28. Garbarz-Glos, B.; Bąk, W.; Kalvane, A.; Antonova, M.; Klimkowski, G. Effects of CuO doping on structure, microstructure and dielectric properties of BaTiO3–PbTiO3 solid solution. *Integrated Ferroelectrics* **2019**, *196*, 70-77, https://doi.org/10.1080/10584587.2019.1591961.
29. Sitko, D.; Bąk, W.; Garbarz-Glos, B.; Budziak, A.; Kajtoch, C.; Kalvane, A. Dielectric properties of BaTiO3 based materials with addition of transition metal ions with variable valence. *IOP Conference Series: Materials Science and Engineering* **2013**, *49*, https://doi.org/10.1088/1757-899X/49/1/012050.
30. Biglar, M.; Gromada, M.; Stachowicz, F.; Trzepieciński, T. Synthesis of Barium Titanate Piezoelectric Ceramics for Multilayer Actuators (MLAs). *Acta Mechanica et Automatica* **2017**, *11*, 275-279, https://doi.org/10.1515/ama-2017-0042.
31. Tao, J.; Cao, S.-a.; Feng, R.; Deng, Y. High dielectric thin films based on barium titanate and cellulose nanofibrils. *RSC Advances* **2020**, *10*, 5758-5765, https://doi.org/10.1039/c9ra10916a.
32. Gao, X.; Li, L.; Jian, J.; Wang, H.; Fan, M.; Huang, J.; Wang, X.; Wang, H. Vertically Aligned Nanocomposite BaTiO3:YMnO3 Thin Films with Room Temperature Multiferroic Properties toward

Nanoscale Memory Devices. *ACS Applied Nano Materials* **2018**, *1*, 2509-2514, https://doi.org/10.1021/acsanm.8b00614.
33. Zheng, T.; Wu, J. Perovskite BiFeO3–BaTiO3 Ferroelectrics: Engineering Properties by Domain Evolution and Thermal Depolarization Modification. *Advanced Electronic Materials* **2020**, *6*, https://doi.org/10.1002/aelm.202000079.
34. Semenov, A.; Dedyk, A.; Mylnikov, I.; Pakhomov, O.; Es'kov, A.; Anokhin, A.; Krylov, V.; Burovikhin, A.; Pavlova, Y.; Tselev, A.; Kholkin, A. Mn-Doped BaTiO3 Ceramics: Thermal and Electrical Properties for Multicaloric Applications. *Materials* **2019**, *12*, 1-9, https://doi.org/10.3390/ma12213592.
35. Yasmm, S.; Choudhury, S.; Hakim, M.A.; Bhuiyan, A.H.; Rahman, M.J. Effect of Cerium Doping on Microstructure and Dielectric Properties of BaTiO3 Ceramics. *Journal of Materials Science & Technology* **2011**, *27*, 759-763, https://doi.org/10.1016/S1005-0302(11)60139-4.
36. Alex, K.V.; Prabhakaran, A.; Jayakrishnan, A.R.; Kamakshi, K.; Silva, J.P.B.; Sekhar, K.C. Charge Coupling Enhanced Photocatalytic Activity of BaTiO3/MoO3 Heterostructures. *ACS Applied Materials & Interfaces* **2019**, *11*, 40114-40124, https://doi.org/10.1021/acsami.9b14919.
37. Rao, M. Effect of Copper Doping on Structural, Dielectric and DC Electrical Resistivity Properties of BaTiO3. *Advances in Materials Physics and Chemistry* **2013**, *3*, 77-82, https://doi.org/10.4236/ampc.2013.31012.
38. Bosman, A.J.; Havinga, E.E. Temperature Dependence of Dielectric Constants of Cubic Ionic Compounds. *Physical Review* **1963**, *129*, 1593-1600, https://doi.org/10.1103/PhysRev.129.1593.
39. Jiang, B.; Iocozzia, J.; Zhao, L.; Zhang, H.; Harn, Y.-W.; Chen, Y.; Lin, Z. Barium titanate at the nanoscale: controlled synthesis and dielectric and ferroelectric properties. *Chemical Society Reviews* **2019**, *48*, 1194-1228, https://doi.org/10.1039/c8cs00583d.
40. Kang, S.; Guo, H.; Wang, J.; Zhong, X.; Li, B. Influence of surface coating on the microstructures and dielectric properties of BaTiO3 ceramic via a cold sintering process. *RSC Advances* **2020**, *10*, 30870-30879, https://doi.org/10.1039/d0ra03849k.
41. Sagdeo, A.; Nagwanshi, A.; Pokhriyal, P.; Sinha, A.K.; Rajput, P.; Mishra, V.; Sagdeo, P.R. Disappearance of dielectric anomaly in spite of presence of structural phase transition in reduced BaTiO3: Effect of defect states within the bandgap. *Journal of Applied Physics* **2018**, *123*, https://doi.org/10.1063/1.5010870.
42. Mostafa, M.; Rahman, M.J.; Choudhury, S. Enhanced dielectric properties of BaTiO3 ceramics with cerium doping, manganese doping and Ce-Mn co-doping. *Science and Engineering of Composite Materials* **2019**, *26*, 62-69, https://doi.org/10.1515/secm-2017-0177.
43. Li, L.; Zhang, D.; Liu, J.; Li, Y. Dielectric properties and microstructure of BaTiO3-SiO2 nanocomposites using vacuum treated barium titanate nanoparticles. *Materials Research Express* **2020**, *6*, https://doi.org/10.1088/2053-1591/ab6a4d.